Supporting Information

Masson et al. 10.1073/pnas.1116772109

SI Materials and Methods

Bacterial Strains and Preparation. We used *Escherichia coli* strain HCB1 for all of the experiments involving aspartate, α-methylaspartate, leucine, and serine and *E. coli* strain MG1655 (see below) for glucose experiments. Experiments were realized using the following protocols for the two strains, respectively. Clones were suspended in LB medium and shaken at 34 °C (37 °C) until saturation was reached. The culture was then diluted 200× in T-broth (100× in LB) and shaken again at 34 °C (37 °C) until the optical density OD 600 nm = 0.3 (0.4) was reached. Bacteria were then centrifuged for 5 min (three times for 10 min) at 2,000 × *g* and resuspended in the motility medium MM (1). Finally, the suspension was further diluted before injection in the experimental setup. ΔCheZ, ΔCheR, and ΔCheRCheB mutants of the MG1655 strain were produced using standard phage P1 transduction protocols.

The sensitivity of our strain HCB1 to glucose was limited, so we considered the strain MG1655 and amplified its sensitivity with a selection on a ring assay. Bacteria were grown on soft agar with glucose. Bacteria moving on the most advanced edge of the ring were selected and grown under the same conditions. The selection was repeated 10 times, yielding the *E. coli* MG1655 strain that we used for the experiments presented here.

Tracking Trajectories. Image analysis was performed with the ImageJ (National Institutes of Health) Particle Tracker plugin (https://weeman.inf.ethz.ch/ParticleTracker). After subtracting the background, images were smoothed and a boundary detection algorithm was applied. Individual trajectories were obtained with a minimum distance association between consecutive frames. The density of bacteria, which we kept deliberately low, prevented mismatched association, so that bacteria could disappear up to 10 frames and still be tracked. Up to 100 bacteria could be tracked in the field of view for acquisition times from 20 to 200 s. Images were taken ∼100 μm above the glass bottom of the setup (about the midplane). Bacteria close to the surface can easily be detected, as they tend to swim parallel to the surface, drawing circular trajectories. A few occasional tracks that displayed this behavior were manually detected and integrally eliminated.

Tumbles were defined on the basis of changes in speed and direction of motion. The rationale is that a tumble is associated with an abrupt change in the direction of motion and/or a very rapid decrease in the velocity of motion. The specific criteria that we used are as follows. Trajectories were first smoothed with a running average over a few points; the instantaneous velocity and the direction of motion were evaluated on the smoothed trajectories. As for the criterion on the velocity, we first detected local minima of the absolute velocity (the location of a generic one is denoted t_{min}). The location of the two closest local maxima is denoted by t_1 and t_2 ($t_1 < t_{min} < t_2$), and we computed the relative change in speed $\Delta v/v(t_{min})$, where the variation $\Delta v = \max[v(t_1) - v(t_{min}), v(t_2) - v(t_{min})]$). If the relative variation was sufficiently large, namely $\Delta v/v(t_{min}) \geq \alpha$ with $\alpha = 0.7$, we considered that the bacterium was in the tumbling state for those subintervals, $\Delta t \in [t_1, t_2]$, where the local velocity $v(t) \leq v(t_{min}) + 0.2\Delta v$. A similar criterion was used for variations in the direction of motion. We first detected local maxima in the absolute value of the angular deviation. The time where a local maximum was achieved is denoted by t_{max} and the two surrounding local minima by t_1 and t_2. If the total change in direction across the interval was sufficiently large with respect to the typical one due to pure rotational diffusivity [$\sum|\Delta\theta| \geq \beta\sqrt{2D_{rot}(t_2 - t_1)}$ with $\beta = 2$ and $D_{rot} = 0.1$ rad^2/s], we considered that the bacterium was in the tumbling state for those subintervals where the angular variation was close to maximal: $|\Delta\theta(t_{max}) - \Delta\theta(t)| \leq 0.2|\Delta\theta(t_{max})|$. We verified manually over a large number of trajectories that these definitions give sensible results, in agreement with visual inspection (Fig. S7).

Microfluidic Setup. Fig. S5 presents the microfluidic setup used for the experiments described in the main text. Fig. S6 shows an image of the concentration field within the channel under stable conditions (*Left*) and a typical sample of bacterial tracks (*Right*).

Likelihood Distributions and Numerical Simulations. Two instances of likelihood distributions for the inferred parameters are presented. The curves are representative of the two classes appearing in the inference procedure. In Fig. S3 (*Left*), the distribution shows a well-defined maximum, whereas other sets of trajectories may display (*Right*) a peaked distribution with a "soft direction" $\alpha_0 \sim \lambda^2$, where a slower decrease is observed. Its origin is discussed in the main text.

Fig. S8 presents two instances of inferred responses to aspartate with the corresponding errors. In Fig. S9, we show the results of a numerical test of the efficiency of the inference procedure on a set of trajectories generated synthetically by using the model described in the next section.

Mathematical Modeling of the Chemotactic Response Function.
Definitions. The intracellular signaling pathway and the ensuing chemotactic motion in response to serine and methylaspartate can be conveniently and accurately summarized by a simple dynamical model that is here recalled for completeness (2–9).

The receptor cluster is described by means of the Monod–Wyman–Changeux allosteric model with activity $a = [\text{CheA}\sim\text{p}]/[\text{CheA}]_{\text{tot}}$. The number of Tar methylaspartate receptors in a cluster is n_a and the number of Tsr serine receptors is n_s. The model can also account for the low-affinity binding of methylaspartate to Tsr and of serine to Tar. Methylation occurs at a rate $F(a,m)$ dependent on activity and methylation. The methyltransferase CheR/methylesterase CheB acts on an assistance neighborhood of 7/5 receptor dimers (10, 4). The mean methylation level per receptor monomer lies in the range $0 \leq m \leq M = 4$ and is considered to be a continuous function. Saturation kinetics of methylation/demethylation is accounted by Michaelis–Menten terms in $F(a,m)$. The linear dependence of the methylation-dependent part of the free energy has been documented in ref. 11. The phosphorylated fraction of CheY is denoted $y = [\text{CheY}\sim\text{p}]/[\text{CheY}]_{\text{tot}}$, and $h(y)$ is the equilibrium probability that the bacterium is running, a decreasing sigmoidal function of y. The rate of CheY∼p dephosphorylation by the phosphatase CheZ is k_z, and k_a is the rate of CheY phosphorylation by the active receptor. Finally, τ_t is the average duration of a tumbling event, assumed to be independent of ligand concentration. Slightly more refined models account for the phosphorylation of CheB by CheA∼p, through the equilibrium expression $[CheB] = [CheB]_{tot}\, a/(a + K_a)$. However, significant deviations from a linear dependence of the methylation rate on the activity are detectable only for large values of the activity [larger than ∼0.7 (11)], characteristic of extremely tumbly motion and therefore largely irrelevant for the present analysis.

Model equations. The model is summarized by the following set of equations:

$$a = G(m, [Ser], [Asp])$$

$$\frac{dm}{dt} = F(a, m)$$

$$\frac{dy}{dt} = k_a a(1-y) - k_z y$$

$$\frac{dp_r}{dt} = \frac{1-(p_r/h(y))}{\tau_t}$$

The detailed expressions for the functions that appear in the previous equations are

$$G(m, [Ser], [Asp]) = (1 + e^{f(m,[Ser],[Asp])})^{-1}$$

$$\begin{aligned} f(m, [Ser], [Asp]) =& (n_a + n_s)\alpha(m_0 - m) \\ &+ n_s \ln \frac{1 + [Ser]/K^{off}_{Ser,Tsr} + [Asp]/K^{off}_{Asp,Tsr}}{1 + [Ser]/K^{on}_{Ser,Tsr} + [Asp]/K^{on}_{Asp,Tsr}} \\ &+ n_a \ln \frac{1 + [Asp]/K^{off}_{Asp,tar} + [Ser]/K^{off}_{Ser,Tar}}{1 + [Asp]/K^{on}_{Asp,tar} + [Ser]/K^{on}_{Ser,Tar}} \end{aligned}$$

$$F(a, m) = k_r[CheR](1-a)\frac{M-m}{M-m+K_R} - k_b[CheB]a\frac{m}{m+K_B}$$

In the free energy, $f(m, [Ser], [Asp])$, both the specific bindings Tar/Asp and Tsr/Ser and the less specific ones Asp/Tsr and Ser/Tar are included. The latter are relevant at comparatively large ligand concentrations.

Amplification of sensitivity through flagellar bundling. The probability of being in a run phase given a certain level of intracellular concentration of CheY∼p, that is, $h(y)$, is set to the probability of having the majority of motors running counterclockwise (CCW). We remark that such an admittedly simplistic "voter model" is used here only for the purpose of illustrating the nontrivial role that can be played by flagellar bundling, without any claim of providing a realistic description of multiple motors/flagella dynamics. Indeed, as shown in ref. 12, even a single clockwise (CW) rotating motor can significantly reorient the cell. The degree of independence of different motors is also not clear. This caveat made, we show that the voter model of the collective flagellar dynamics could provide an additional degree of amplification. Validation of this hypothesis would require a detailed model including motor switching, correlations among motors, and hydrodynamic interactions, beyond the scope of the present work. The single motor has a probability of CCW rotation given by $h_s(y) = [1 + (y/y_0)^H]^{-1}$, with $H = 10$ (13); therefore, if $n = 6$ is an average number of motors, the explicit expression for the run probability is simply

$$h(y) = h_s(y)^6 + 6h_s(y)^5(1-h_s(y)) + 15h_s(y)^4(1-h_s(y))^2$$

As a consequence of this cooperation, the slope of the curve $h(y)$ around the equilibrium value is significantly larger (about six times) than the slope of the single-motor probability $h_s(y)$. This leads to a corresponding increase in the sensitivity of bacteria to changes in attractant concentration.

Parameters. The parameters used in the numerical simulations are listed in Table S1.

Chemotactic response function. In the linear response regime, any change in concentration can be decomposed as the superposition of responses to elementary stimuli. Therefore, as we shall see, it is sufficient to focus attention on the response to impulsive changes in concentration.

For mild variations of chemoattractant concentration around a uniform level, that is, in the linear response limit, the evolution of the running probability takes the customary form of a two-state inhomogeneous Poisson process,

$$\frac{dp_r}{dt} = \frac{1}{\tau_t}(1-p_r) - \frac{1}{\tau_t\left(\frac{h}{1-h}\right)}p_r.$$

Then, developing to first-order around the equilibrium value, denoted by an asterisk, one obtains

$$\frac{dp_r}{dt} = \frac{1}{\tau_t}(1-p_r) - \frac{1}{\tau_r^*}\left(1 - \frac{h'^*\Delta y}{h^*(1-h^*)}\right)p_r \text{ with}$$

$$\tau_r^* = \tau_t\frac{h^*}{1-h^*}, \text{ and } h'^* = \frac{dh^*(y)}{dy}.$$

The modulation of the rate of conversion from run to tumble when the bacterium is exposed to a variable ligand concentration L then reads

$$Q(t) \equiv \frac{h'_*\Delta y(t)}{h_*(1-h_*)} = \int_{-\infty}^{t} K(t-t')L(t')dt',$$

whereby we have introduced the linear response function $K(t)$ to an impulsive change in attractant. If $L(t) = \Delta L \cdot \delta(t)$, then the response reads

$$K(t) = \frac{h'^*\Delta y(t)}{h^*(1-h^*)\Delta L}.$$

The explicit form of this response function is obtained by integrating the equations (for the sake of simplicity, only specific ligand/receptor binding is considered):

$$\begin{aligned} \frac{d\Delta p_r(t)}{dt} &= -\frac{(\Delta p_r(t) - \Delta y(t)h'^*p_r^*/h^*)}{\tau_t h^*} \\ &= -\frac{\Delta p_r(t)}{\tilde{\tau}} + \frac{1}{\tau_t}\frac{h'^*}{h^*}\Delta y(t) \\ \frac{d\Delta y(t)}{dt} &= k_a(1-y^*)\left(\frac{\partial G}{\partial m}\right)^*\Delta m(t) - (k_z + k_a a^*)\ \Delta y(t) \\ &= k_a(1-y^*)\left(\frac{\partial G}{\partial m}\right)^*\Delta m(t) - \frac{\Delta y(t)}{\tau_y} \\ \frac{d\Delta m(t)}{dt} &= \left(\frac{\partial F}{\partial a}\frac{\partial G}{\partial m} + \frac{\partial F}{\partial m}\right)^*\Delta m(t) = -\frac{\Delta m(t)}{\tau_m} \end{aligned}$$

with $\frac{1}{\tilde{\tau}} = \frac{1}{\tau_r^*} + \frac{1}{\tau_t}$, $\tau_y = \frac{1}{k_z + k_a a^*}$, and $\tau_m = \left(\frac{\partial F}{\partial a}\frac{\partial G}{\partial m} + \frac{\partial F}{\partial m}\right)^{*-1}$, supplemented by the initial conditions

$$\begin{aligned} \Delta m(0) &= \left(\frac{\partial F}{\partial a}\frac{\partial G}{\partial L}\right)^*\Delta L \\ \Delta y(0) &= k_a(1-y^*)\left(\frac{\partial G}{\partial L}\right)^*\Delta L \\ \Delta p_r(0) &= 0 \end{aligned}$$

that correspond to an impulsive stimulus $\Delta L\delta(t)$. The explicit expressions for the various partial derivatives appearing in the previous formulas are

$$\left(\frac{\partial F}{\partial a}\right)^* = -k_r[CheR]\frac{M-m^*}{M-m^*+K_R} - k_b[CheB]\frac{m^*}{m^*+K_B} < 0$$

$$\left(\frac{\partial F}{\partial m}\right)^* = -(1-a^*)k_r[CheR]\frac{K_R}{(M-m^*+K_R)^2} - a^*k_b[CheB]\frac{K_B}{(m^*+K_B)^2} \le 0$$

$$\left(\frac{\partial G}{\partial m}\right)^* = a^*(1-a^*)\alpha(n_a+n_s) > 0$$

$$\left(\frac{\partial G}{\partial L}\right)^* = -a^*(1-a^*)n_s\left(\frac{(K^{off})^{-1}}{1+\frac{L}{K^{off}}} - \frac{(K^{on})^{-1}}{1+\frac{L}{K^{on}}}\right)$$

The solution reads

$$\Delta m(t) = \Delta m(0)e^{-t/\tau_m}$$

$$\Delta y(t) = \Delta y(0)e^{-t/\tau_y} + k_a(1-y^*)\left(\frac{\partial G}{\partial m}\right)^*\Delta m(0)\frac{e^{-t/\tau_m}-e^{-t/\tau_y}}{\tau_y^{-1}-\tau_m^{-1}}$$

$$\Delta p_r(t) = \frac{1}{\tau_t}\frac{h'^*}{h^*}\left[\Delta y(0)\left(\frac{e^{-t/\tau_y}-e^{-t/\tilde{\tau}}}{\tilde{\tau}^{-1}-\tau_y^{-1}}\right) + k_a(1-y^*)\left(\frac{\partial G}{\partial m}\right)^* \times \Delta m(0)\left(\frac{e^{-t/\tau_y}}{(\tau_y^{-1}-\tau_m^{-1})(\tau_y^{-1}-\tilde{\tau}^{-1})} + \frac{e^{-t/\tau_m}}{(\tau_m^{-1}-\tau_y^{-1})(\tau_m^{-1}-\tilde{\tau}^{-1})} + \frac{e^{-t/\tilde{\tau}}}{(\tilde{\tau}^{-1}-\tau_y^{-1})(\tilde{\tau}^{-1}-\tau_m^{-1})}\right)\right]$$

whence the result, for example, for the response to an impulsive stimulus of ligand,

$$K(t) = k_a\frac{h'^*(1-y^*)}{h^*(1-h^*)}\left(\frac{\partial G}{\partial L}\right)^*(\tau_y^{-1}-\tau_m^{-1})^{-1} \times\left[\left(\tau_y^{-1}e^{-t/\tau_y}-\tau_m^{-1}e^{-t/\tau_m}\right) - \left(\frac{\partial F}{\partial m}\right)^*\left(e^{-t/\tau_m}-e^{-t/\tau_y}\right)\right]$$

The response is the sum of two exponentials and is here decomposed into two contributions: The first term inside the square brackets integrates to zero, whereas the second one, proportional to $(\frac{\partial F}{\partial m})^*$, evaluates at zero at the time of impulsive stimulation.

When the response function is written in the form $K(t) = A_y e^{-\lambda_y t} + A_m e^{-\lambda_m t}$, the biochemical parameters are $\tau_y^{-1} = \lambda_y$, $\tau_m^{-1} = \lambda_m$, $k_a\frac{h'^*(1-y^*)}{h^*(1-h^*)}(\frac{\partial G}{\partial L})^* = A_y + A_m$, $(\frac{\partial F}{\partial m})^* = -(\frac{A_m\lambda_y + A_y\lambda_m}{A_m + A_y})$.

From the Response Function to the Bias Response. In the tethering assay, the bias response function is defined as the fraction of bacteria whose flagellum turns CCW following an impulse stimulus (14). In our framework, the bias response reads $K_b(t) \equiv \Delta p_r(t)/\Delta L$. From the definition of the response function $K(t) = \frac{h'^*\Delta y(t)}{h^*(1-h^*)\Delta L}$, the linearized equation for the variation of the bias $\frac{d\Delta p_r(t)}{dt} = -\frac{\Delta p_r(t)}{\tilde{\tau}} + \frac{1-h^*}{\tau_t}K(t)\Delta L$ is readily integrated to give $K_b(t) = \frac{1-h_*}{\tau_t}\int_0^t K(t')e^{-(t-t')/\tilde{\tau}}dt'$.

This expression shows that, although the response $K(t)$ does not vanish at $t = 0$, the bias response always starts from zero. Therefore, the Laguerre expansion of $K_b(t)$ only features polynomials of order larger than one, whereas the expansion of $K(t)$ starts with a zero-order polynomial, that is, the constant. [The response $K(t)$ itself has in fact a delay introduced by the receptors' time of switching between their two possible forms. However, this time is on the order of milliseconds and therefore not relevant for the timescales analyzed here.] Because $K_b(t)$ was the curve to be reproduced in ref. 15, the development in Laguerre polynomials of $K_b(t)$ was started directly with the linear term. Having now the curves $K(t)$ experimentally measured, theoretical arguments can be developed directly on the response function $K(t)$. Its development starts with the constant term as $K(t) = e^{-\lambda t}(\alpha_0 - \alpha_1\lambda t)$, and the same optimization procedure as in ref. 15 is applied. One then obtains adaptation, that is, $\alpha_0 = \alpha_1$, the optimal values $\tau_r = 1/(3D_{rot}) \approx 1.3s$, and $\lambda = 4D_{rot} \approx 1s^{-1}$, and the corresponding optimal response curve shown in Fig. S4, which compares well with typical experimental curves.

Notice also that if the time integral of K vanishes, the integral over the bias response vanishes as well. The comparison between the bias response to aspartate as inferred by the present method and the one measured in ref. 14 is shown in Fig. 2*D* of the main text.

Sensitivity and Adaptation. The behavior of the chemotactic response is characterized by two quantities that naturally emerge when considering the response to a small step in attractant concentration: its *sensitivity* to fold changes and its *precision* of adaptation (or its inverse, the *error* of adaptation). These are defined as follows (Fig. S1). The input is the chemoattractant concentration, $I = L$, and the output is $O = \tau_r/(1-Q(t))$, that is, the inverse of the instantaneous rate of conversion from run to tumble or, equivalently, in the linear regime $O = \tau_r(1 + \Delta L\int_0^t K(t')dt')$. Denoting by I_1 and O_1 the initial, equilibrium values of the input and output, respectively, by I_2 and O_2 the final values, and O_{peak} the maximum value of the output, one defines

$$\text{Sensitivity} = S = \left|\frac{(O_{peak}-O_1)/O_1}{(I_2-I_1)/I_1}\right| = L\int_0^{t_{peak}}K(t)dt$$

$$\text{Error} = E = \frac{(O_2-O_1)/O_1}{(I_2-I_1)/I_1} = L\int_0^{\infty}K(t)dt$$

$$\text{Precision} = P = |E|^{-1},$$

where we used $(O_{peak}-O_1)/O_1 = \Delta L\int_0^{t_{peak}}K(t)dt$ and $(I_2-I_1)/I_1 = \Delta L/L$. Above, t_{peak} is the time when the response to a step impulse is maximal. By differentiating the integral of the impulse response, it is easy to see that $K(t_{peak}) = 0$, giving $t_{peak} = (\tau_y^{-1}-\tau_m^{-1})\ln\{[\tau_y^{-1} + (\partial F/\partial m)_*]/[\tau_m^{-1} + (\partial F/\partial m)_*]\}$ or, in terms of the output parameters of the inference procedure, $t_{peak} = \frac{\alpha_0}{\alpha_1\lambda}$. As for the error, one has $E = L(A_m\lambda_m^{-1} + A_y\lambda_y^{-1})$. Both sensitivity and precision are approximately independent of ligand concentration in the range $K_{off} \ll L \ll K_{on}$ of ligand concentrations (Fig. S2).

1. Berg HC, Brown DA (1972) Chemotaxis in *Escherichia coli* analysed by three-dimensional tracking. *Nature* 239:500–504.
2. Mello BA, Tu Y (2005) An allosteric model for heterogeneous receptor complexes: Understanding bacterial chemotaxis responses to multiple stimuli. *Proc Natl Acad Sci USA* 102:17354–17359.
3. Keymer JE, Endres RG, Skoge M, Meir Y, Wingreen NS (2006) Chemosensing in *Escherichia coli*: Two regimes of two-state receptors. *Proc Natl Acad Sci USA* 103: 1786–1791.
4. Hansen CH, Endres RG, Wingreen NS (2008) Chemotaxis in *Escherichia coli*: A molecular model for robust precise adaptation. *PLoS Comput Biol* 4:e1.
5. Emonet T, Cluzel P (2008) Relationship between cellular response and behavioral variability in bacterial chemotaxis. *Proc Natl Acad Sci USA* 105:3304–3309.
6. Tu Y, Shimizu TS, Berg HC (2008) Modeling the chemotactic response of *Escherichia coli* to time-varying stimuli. *Proc Natl Acad Sci USA* 105:14855–14860.
7. Vladimirov N, Løvdok L, Lebiedz D, Sourjik V (2008) Dependence of bacterial chemotaxis on gradient shape and adaptation rate. *PLoS Comput Biol* 4:e1000242.
8. Jiang L, Ouyang Q, Tu Y (2009) A mechanism for precision-sensing via a gradient-sensing pathway: A model of *Escherichia coli* thermotaxis. *Biophys J* 97(1):74–82.
9. Vladimirov N, Lebiedz D, Sourjik V (2010) Predicted auxiliary navigation mechanism of peritrichously flagellated chemotactic bacteria. *PLoS Comput Biol* 6:e1000717.
10. Li M, Hazelbauer GL (2005) Adaptational assistance in clusters of bacterial chemoreceptors. *Mol Microbiol* 56:1617–1626.
11. Shimizu TS, Tu Y, Berg HC (2010) A modular gradient-sensing network for chemotaxis in *Escherichia coli* revealed by responses to time-varying stimuli. *Mol Syst Biol* 6:382.

12. Turner L, Ryu WS, Berg HC (2000) Real-time imaging of fluorescent flagellar filaments. *J Bacteriol* 182:2793–2801.
13. Cluzel P, Surette MG, Leibler S (2000) An ultrasensitive bacterial motor revealed by monitoring signaling proteins in single cells. *Science* 287:1652–1655.
14. Segall JE, Block SM, Berg HC (1986) Temporal comparisons in bacterial chemotaxis. *Proc Natl Acad Sci USA* 83:8987–8991.
15. Celani A, Vergassola M (2010) Bacterial strategies for chemotaxis response. *Proc Natl Acad Sci USA* 107:1391–1396.

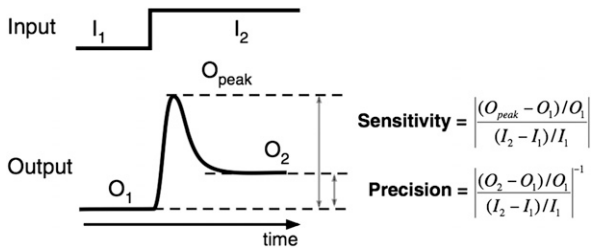

Fig. S1. Definitions of the sensitivity and the precision of the response. The input is the ligand concentration $L(t)$ (a step in the case shown here) and the output is the instantaneous run time $O = \tau_{r,*}/(1-Q(t))$.

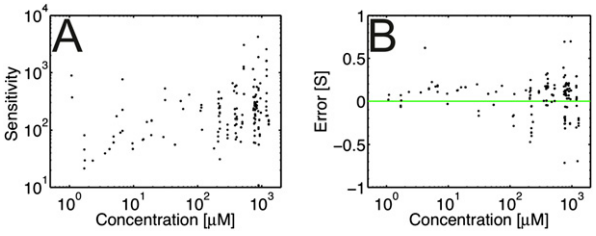

Fig. S2. (*A*) Sensitivity of the response $S = L\int_0^{t_{peak}} K(t)dt$ versus the background α-methylaspartate (MeAsp) concentration L. (*B*) Error of adaptation $E = L\int_0^{\infty} K(t)dt$ versus the concentrations of MeAsp. The green line corresponds to perfect adaptation.

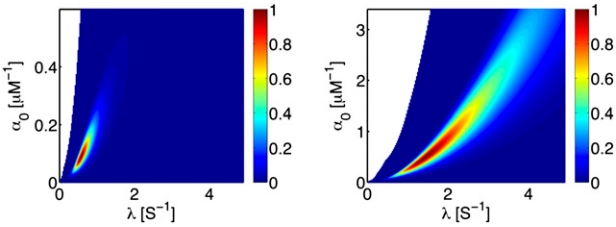

Fig. S3. The likelihood for the two parameters $\{\alpha_0, \lambda\}$ of an adapted response function, that is, $\alpha_1 = \alpha_0$, is shown. The color code is on the right. Note the direction of slow decay (*Right*), whose direction agrees with the arguments discussed in the body of the paper. The white areas on the left side of the graphs correspond to parameter values where the likelihood is not defined (those values generate inconsistencies in the trajectories, e.g., negative probabilities).

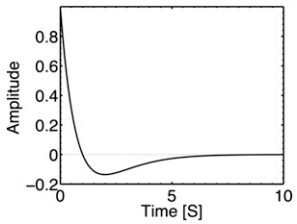

Fig. S4. Optimal response function, as predicted by the arguments presented in ref. 15.

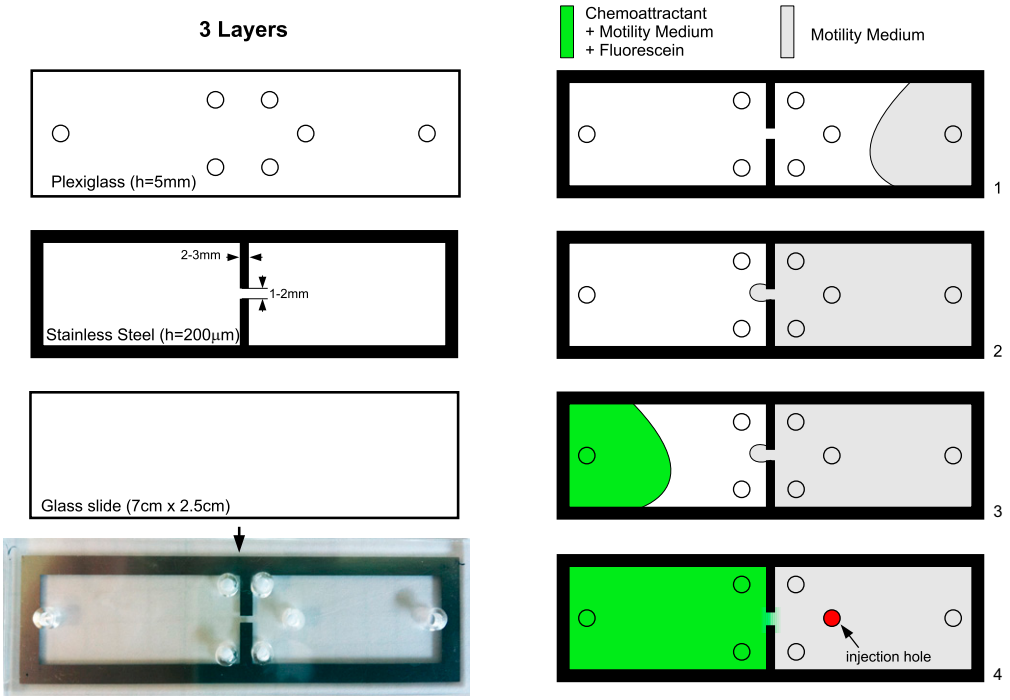

Fig. S5. The chemotaxis setup was designed so as to obtain a stable concentration gradient of chemoattractant without any flow. The gradient is established through diffusion between two large reservoirs to obtain a stable equilibrium. (*Left*) The setup is obtained by superposing a glass slide, a thin (200-μm height) inox steel piece (STEEC) that separates the reservoirs by a channel 1-mm wide and 3-mm long, and a Plexiglas slide with filling holes. The three pieces are insulated with vacuum grease, and a photo of the experimental setup is shown. (*Right*) After sequential filling of the chambers, a stable gradient is established in about 2 h, consistently with attractant (and repellent) diffusion coefficients on the order of 100 $\mu m^2/s$. A small volume (1 μL) of suspension is then injected. The ensuing perturbation slightly alters the gradient, which recovers in a few minutes. The resulting stationary state is stable for about 4 h.

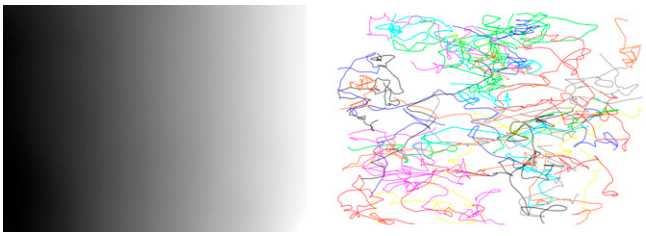

Fig. S6. (*Left*) Normalized intensity of fluorescein gradient inside the channel. (*Right*) Results of a 100-s data acquisition. We display 51 tracks, marked by different colors. Only trajectories with residence time in the field of view longer than 20 s are shown.

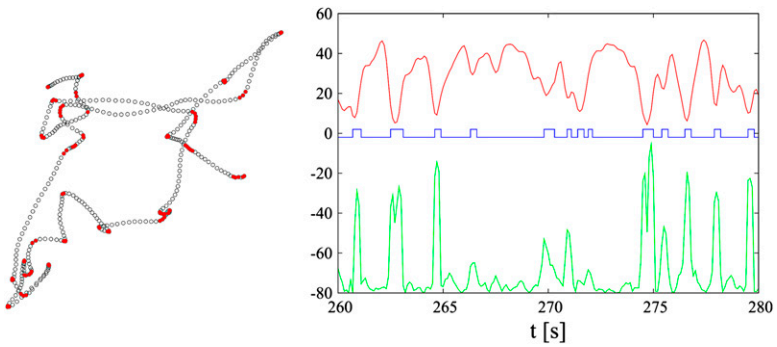

Fig. S7. (*Left*) An individual experimental trajectory. Run phases are represented by empty circles, whereas tumbles are indicated by filled red circles. (*Right*) A snapshot of 20 s of the trajectory on the left is shown to indicate tumble detections. Absolute instantaneous speed (red line, in μm/s), angular variation (green curve, in degrees per frame, vertically shifted by −80°), and detected tumble phases (blue line, arbitrary units, positive for tumbles, negative for runs) are shown.

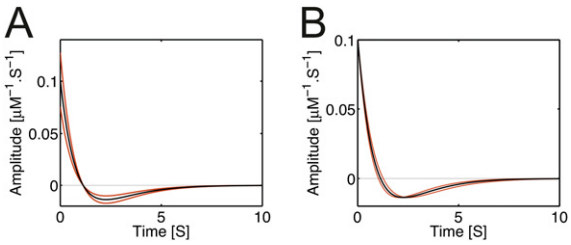

Fig. S8. (*A*) A chemotactic response (black), with the two curves shown in red corresponding to the standard deviations of the error on the estimation of the amplitude. (*B*) The same as in *A*, but the standard deviates are now for the error of the estimation of the memory parameter λ, which affects the decay rate and the shape of the response function.

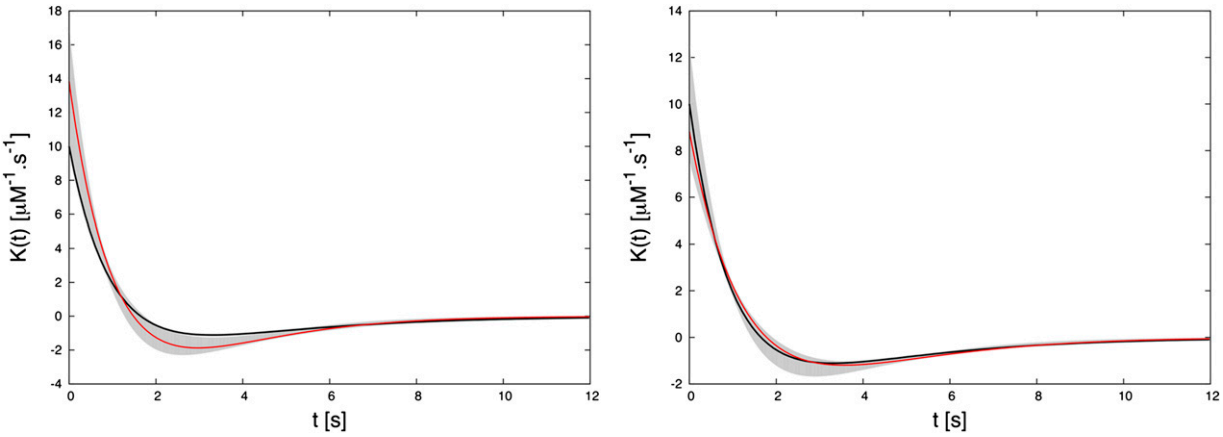

Fig. S9. Test of the inference procedure on synthetic trajectories numerically generated by integration of the model equations. The exact chemotactic response used to generate the trajectories is shown in black. In red, the inferred response from 10 (*Left*) and 50 (*Right*) trajectories of duration 100 s. The gray envelope shows the statistical error in the inference procedure estimated by computing the local curvature of the likelihood profile at the maximum.

Table S1. Values of the parameters used in the computational model

$K^a_{Tar,off}$	5 μM	$K^a_{Tar,on}$	160 μM
$K^s_{Tar,off}$	7 mM	$K^s_{Tar,on}$	10 M
$K^s_{Tsr,off}$	1.8 μM	$K^s_{Tsr,on}$	120 μM
$K^a_{Tsr,off}$	10 mM	$K^a_{Tsr,on}$	1 M
α	0.5	m_0	2
n_a	6	n_s	12
$k_r[CheR]$	0.2 s^{-1}	$k_b[CheB]$	0.4 s^{-1}
k_a	3.0 s^{-1}	k_z	2.0 s^{-1}
H	10	$\tau_{r,*}$	1.0 s
τ_t	0.25 s	v	20 μm/s
D_{rot}	0.25 rad^2/s	y_0	0.35
N	7		

The response $K(t)$ itself has in fact a delay introduced by the receptors' time of switching between their two possible forms. However, that time is on the order of ms and therefore not relevant for the time scales analyzed here.